The Journal of Immunology

RESEARCH ARTICLE | MARCH 08 2023

Identification of a Double-β-Defensin with Multiple Antimicrobial Activities in a Marine Invertebrate FREE

Bang Xiao; ... et. al

J Immunol (2023) 210 (9): 1324–1337.
https://doi.org/10.4049/jimmunol.2200817

Identification of a Double-β-Defensin with Multiple Antimicrobial Activities in a Marine Invertebrate

Bang Xiao,*,† Yue Wang,*,† Danrong Xian,*,† Taolin Fan,*,† Jianguo He,*,†,‡,§ and Chaozheng Li*,†,‡,§

β-Defensins are a family of cysteine-rich antimicrobial peptides that are generally monodomain. Interestingly, the avian β-defensin 11 (AvBD11) is unique, with two β-defensin motifs with a broad range of antimicrobial activities. However, a double-sized β-defensin has not been identified and functionally characterized in invertebrates. In this study, we cloned and identified a double-β-defensin in shrimp *Litopenaeus vannamei* (named LvDBD) and explored its potential roles during infection with shrimp pathogens *Vibrio parahaemolyticus* and white spot syndrome virus (WSSV). LvDBD is an atypical double-sized defensin, which is predicted to possess two motifs related to β-defensin and six disulfide bridges. The RNA interference–mediated knockdown of LvDBD in vivo results in phenotypes with increased bacterial loads, rendering the shrimp more susceptible to *V. parahaemolyticus* infection, which could be rescued by the injection of recombinant LvDBD protein. In vitro, rLvDBD could destroy bacterial membranes and enhance hemocyte phagocytosis, possibly attributable to its affinity to the bacterial wall components LPS and peptidoglycan. In addition, LvDBD could interact with several viral envelope proteins to inhibit WSSV proliferation. Finally, the NF-κB transcription factors (Dorsal and Relish) participated in the regulation of LvDBD expression. Taken together, these results extend the functional understanding of a double-β-defensin to an invertebrate and suggest that LvDBD may be an alternative agent for the prevention and treatment of diseases caused by *V. parahaemolyticus* and WSSV in shrimp. ***The Journal of Immunology*****, 2023, 210: 1324–1337.**

Invertebrates rely solely on innate immune responses to control and clear invading pathogens. Antimicrobial peptides serve as the first line of defense in innate immunity against a large spectrum of pathogens, such as bacteria, fungi, parasites, and viruses (1). The primary function of antimicrobial peptides is the direct killing or inhibition of invading pathogens. Generally, the antimicrobial mechanism of most antimicrobial peptides involves membrane disruption via their direct interaction with certain membrane constituents (2, 3). In some cases, the hydrophilic and hydrophobic regions of an antimicrobial peptide confer the ability to bind both lipid components and phospholipid groups of the microbial membrane, causing the disintegration of the lipid bilayer structure (4, 5).

β-Defensins are a class of antimicrobial peptides characterized by a conserved β-sheet-rich fold stabilized with three pairs of intramolecular disulfide bridges by six conserved cysteine residues that are linked in the 1–5, 2–4, and 3–6 pattern (6, 7). β-Defensins are ubiquitous and present in all vertebrates but only in some invertebrates. For example, in a recent study, a native form β-defensin-like peptide from *Homarus americanus* was identified and characterized by mass spectrometry (8). Among vertebrate defensins, the family of avian β-defensin 11 (AvBD11) has a unique structure composed of two β-defensin domains by the typical disulfide array Cys1–Cys5, Cys2–Cys4, and Cys3–Cys6 (9). These "polydefensins" have not been reported in mammals. The reasons for the emergence of such polydefensins during evolution in particular lineages of vertebrates and functional gain over conventional "monodefensins" have not been fully determined (10). *Gga*-AvBD11 was richly detected in the chicken egg and embryo, and it possessed broad antimicrobial activity against Gram-positive and -negative bacteria, parasites, and viruses (9, 11). Besides, the N-terminal domain of *Gga*-AvBD11 mediated antibacterial and antiparasitic activities; notably, the antiviral activity requires the full-length protein, and the role of the C-terminal domain of *Gga*-AvBD11 remains unclear (9). However, only a few double-β-defensins have been discovered or reported in invertebrates, and their antimicrobial function has not been elucidated.

The shrimp *Litopenaeus vannamei* (Arthropoda, Crustacea, Decapoda, and Penaeidae) has become one of the most important farmed species in the world. Considering the high-density

*Southern Marine Science and Engineering Guangdong Laboratory (Zhuhai)/State Key Laboratory of Biocontrol, School of Marine Sciences, Sun Yat-sen University, Guangzhou, P. R. China; †Guangdong Provincial Key Laboratory of Marine Resources and Coastal Engineering/Guangdong Provincial Key Laboratory for Aquatic Economic Animals, Sun Yat-sen University, Guangzhou, P. R. China; ‡Guangdong Laboratory for Lingnan Modern Agriculture, Maoming, P. R. China; and §China-ASEAN Belt and Road Joint Laboratory on Marine Aquaculture Technology, Guangzhou, P. R. China

ORCIDs: 0000-0001-7393-4048 (Y.W.); 0000-0003-3534-4471 (D.X.); 0000-0001-7639-7831 (C.L.).

Received for publication November 9, 2022. Accepted for publication February 5, 2023.

This work was supported by the National Natural Science Foundation of China (32022085/31930113), the National Key Research and Development Program of China (2022YFD2400204), the open competition program of top 10 critical priorities of Agricultural Science and Technology Innovation Program for the 14th Five-Year Plan of Guangdong Province (2022SDZG01), the Southern Marine Science and Engineering Guangdong Laboratory (Zhuhai) (SML2021SP301), and the Fundamental Research Funds for the Central Universities, Sun Yat-sen University (22lglj05). The funders had no role in study design, data collection and analysis, decision to publish, or preparation of the manuscript.

The sequence presented in this article has been submitted to GenBank (https://www.ncbi.nlm.nih.gov/nuccore/ON081627) under accession number ON081627.

C.L. and J.H. conceived and designed the experiments. B.X., Y.W., D.X., and T.F. performed the experiments and analyzed data. B.X., J.H., and C.L. wrote the draft manuscript. C.L. and J.H. acquired finding. C.L. was responsible for forming the hypothesis; project development; data coordination; and writing, finalizing, and submitting the manuscript. All authors discussed the results and approved the final version.

Address correspondence and reprint requests to Prof. Chaozheng Li or Prof. Jianguo He, School of Marine Sciences, Sun Yat-sen University, Guangzhou, 510275, P. R. China (C.L.) or School of Life Sciences, Sun Yat-sen University, Guangzhou, 510275, P. R. China (J.H.). E-mail addresses: lichaozh@mail2.sysu.edu.cn (C.L.) or lsshjg@mail.sysu.edu.cn (J.H.)

The online version of this article contains supplemental material.

Abbreviations used in this article: AvBD11, avian β-defensin 11; LB, Luria broth; MIC, minimum inhibitory concentration; PGN, peptidoglycan; RNAi, RNA interference; TEM, transmission electron microscopy; UTR, untranslated region; VP, viral envelope protein; WSSV, white spot syndrome virus.

tolerance and rapid growth rate of *L. vannamei*, it has dominated over 80% of global shrimp production each year (12). With the enlargement of the cultivation scale, shrimp farming has been threatened by multiple disease risks. Highly virulent shrimp pathogens, especially *V. parahaemolyticus* and white spot syndrome virus (WSSV), have caused considerable economic losses in the shrimp aquaculture industry worldwide (12). The bacteria *V. parahaemolyticus*, which carries a virulence plasmid of PirA/B, leads to a severe disease in farmed shrimp known as "acute hepatopancreatic necrosis disease" (13). WSSV is a bacilliform, nonoccluded enveloped virus (14), which has an extremely wide host range with up to 98 species and can cause 100% mortality within 7–10 d after viral infection (15). Antibiotic abuse in shrimp aquaculture for the control of bacterial diseases has caused severe threats to the ecological environment and human health (16, 17). Therefore, an environmentally friendly and effective prevention method is urgently needed for diseases, especially those caused by *V. parahaemolyticus* and WSSV.

The presence of two β-defensin motifs in an antimicrobial peptide is rare in vertebrates and invertebrates. In the present study, we identified a two–β-defensin-like peptide from *L. vannamei*, abbreviated LvDBD, which was regulated by the NF-κB pathway. LvDBD has potential antibacterial activity with ability to bind to bacteria and destroy bacterial membrane structure. It could inhibit WSSV infection by interacting with the viral envelope proteins (VPs), including VP19, VP24, VP26, and VP28. Together, our findings extend the functional understanding of a double-β-defensin to an invertebrate, and the LvDBD may be an alternative therapeutic agent to develop for the prevention and treatment of diseases caused by *V. parahaemolyticus* and WSSV in shrimp.

Materials and Methods

Animals and pathogens

Healthy *L. vannamei* (average 5 g each) used in experiments were specific pathogen-free and obtained from the Hai Xingnong Company shrimp farm in Maoming, Guangdong Province, China, and were cultured in a recirculating water tank system filled with air-pumped seawater with 25‰ salinity at 27°C and fed to satiation three times per day with a commercial diet. Gram-negative bacteria, including *V. parahaemolyticus* (ATCC17802), *Aeromonas hydrophila* (ATCC35654), *Pseudomonas aeruginosa* (ATCC27853), and *Escherichia coli* (ATCC25922), and Gram-positive bacteria, including *Staphylococcus aureus* (ATCC29213), *Enterococcus faecalis* (ATCC29212), *Micrococcus luteus* (ATCC49732), and *Bacillus subtilis* (ATCC6633), were purchased from Guangdong Microbial Culture Collection Center and cultured in Luria broth (LB) medium overnight at 37°C. The numbers of bacteria were quantified by counting the microbial CFUs per milliliter on LB agar plates. The final injection concentration of bacteria (*V. parahaemolyticus*) should be controlled to yield ~1×10^5 CFU/50 μl (18).

Cloning of full-length cDNA sequence of LvDBD

Based on the *L. vannamei* transcriptome data in our laboratory (19), a partial cDNA sequence was obtained to amplify the full-length cDNA sequence using the RACE method according to a previously published method (20). In brief, RACE PCR and nested PCR were performed using a SMARTer RACE cDNA amplification kit (Clontech, Dalian, China) in accordance with the manufacturer's instructions. The final PCR products were cloned into the pMD-19T cloning vector (Takara, Dalian, China), and eight positive clones were selected and sequenced. The transcription starting site of LvDBD was determined according to the 5′-RACE PCR amplification. Primer sequences are listed in Table I.

Sequence and phylogenetic analysis

The open reading frame of the cDNA and the deduced amino acids of LvDBD were predicted by using the EditSeq software from DNAStar. The functional domains of proteins were predicted through the Simple Modular Architecture Research Tool (21). ExPASy software (22) was used to predict the protein molecular mass and isoelectric point values. The neighbor-joining phylogenic tree was constructed on the basis of deduced amino acid sequences of LvDBD by using MEGA 5.0 software with 1000 bootstrap replications (23). The three-dimensional models of LvDBD protein were generated by SWISS-MODEL online (https://swissmodel.expasy.org) (24). The structure of LvDBD-FL (full length), LvDBD-N (N-terminal), and LvDBD-C (C-terminal) were predicted by SWISS-MODEL by using the structure of *Gallus gallus* β-defensin 11 (SMTL ID: 6qeu.1) and *Mus musculus* β-defensin 7 (SMTL ID: 1e4t.1).

Total RNA extraction and cDNA synthesis

Total RNA was extracted from different tissues of shrimp using the Eastep Super Total RNA Extraction Kit (Promega, Shanghai, China). The genomic DNA of shrimp tissues was extracted using a genomic DNA extraction kit (Ω, Guangzhou, China). First-strand cDNA synthesis was performed using a cDNA synthesis kit (Takara, Dalian, China).

Tissue expression and immune challenge analysis by quantitative PCR

The relative expression levels of LvDBD were determined by quantitative PCR. For tissue expression distribution, shrimp tissues of eyestalk, epidermis, stomach, gill, heart, hepatopancreas, antenna, intestine, nerve, appendage, and muscle, as well as hemocytes, were sampled and pooled from 15 shrimp. For immune stimulation, the treated groups were injected with 5 μg LPS, 5 μg polyinosinic-polycytidylic acid, 50 μl *V. parahaemolyticus* suspension (~1×10^5 CFU), 50 μl *S. aureus* suspension (~1×10^5 CFU), or 50 μl WSSV (~1×10^5 copies) at the second abdominal segment of each shrimp, and the control group was injected with PBS solution. Hemocytes of challenged shrimps were collected at 0, 4, 8, 12, 24, 36, 48, and 72 h after injection, and the samples at each time point were pooled from 15 shrimp. Total RNA extraction and quantitative PCR were performed as described previously (25). Expression levels of LvDBD were calculated using the Livak ($2^{-\Delta\Delta CT}$) method after normalization to *L. vannamei EF-1α* (https://www.ncbi.nlm.nih.gov/nuccore/GU136229). Primer sequences are listed in Table I.

Recombinant protein expression and purification

The coding sequence of LvDBD (without the signal peptide, 1–18 aa) was amplified by PCR using corresponding primers (Table I) and subcloned into pET-32a(+) plasmid (Merck Millipore, Darmstadt, Germany). After confirmation by sequencing, the recombinant plasmid was transferred into *E. coli* Rosetta (DE3) cells (TransGen Biotech, Beijing, China). Then, positive clones harboring the desired fragment were selected for inducing expression. After 4 h of induction with 0.1 mM isopropyl β-D-thiogalactoside at 30°C, cells were pelleted by centrifugation and sonicated for 30 min in ice water. The supernatant from the sonicated proteins was purified by using Ni-NTA agarose (Qiagen, Düsseldorf, Germany) according to the manufacturer's instructions. The rLvDBD (full length), rLvDBD-N (N-terminal), rLvDBD-C (C-terminal), and rTrx-His-tag was induced and purified in the same way. The purified rLvDBD, rLvDBD-N, rLvDBD-C, and rTrx-His-tag proteins were checked by Coomassie staining or Western blot analysis. The concentration of the purified proteins was determined using a bicinchoninic acid protein assay kit (Beyotime Biotechnology, Shanghai, China).

SDS-PAGE and Western blot analysis

The purified rLvDBD and rTrx-His-tag were analyzed by SDS-PAGE gels and Western blot analysis, and then the proteins were separated on 12.5% SDS-PAGE gels and then transferred to polyvinylidene difluoride membranes (Merck Millipore). After blocking with 5% nonfat milk diluted in TBST buffer (150 mM NaCl, 0.1% Tween-20, 50 mM Tris-HCl, pH 8.0) for 1 h, and the membrane was incubated with 1:1000 mouse anti-6×-His (Sigma-Aldrich, St. Louis, MO) for 2 h at 25°C. The polyvinylidene difluoride membranes were washed three times with TBST and then incubated with 1:2000 goat anti-mouse IgG (H+ L) HRP secondary Ab (Promega) for 1 h. Membranes were developed using an ECL blotting substrate (Thermo Fisher Scientific, Waltham, MA), and the chemiluminescent signal was detected using the 5200 Chemiluminescence Imaging System (Tanon, Shanghai, China).

Pull-down assays

Pull-down assays were performed to explore whether the recombinant rLvDBD could interact with the main envelope proteins of WSSV (VP19, VP24, VP26, and VP28). The recombinant GST-tagged VP19, VP24, VP26, and VP28 were obtained from our previous studies (26). For GST pull-down assays, 5 μg rLvDBD was incubated with 5 μg of GST-tagged WSSV protein solution at 4°C for 3 h by agitation. Subsequently, 20 μl of the GST resin were added, and the agitation continued for another 2 h. The resin was washed four times with PBS. Finally, the resins were resuspended in 50 μl of the SDS-PAGE sample buffer, boiled, and analyzed by Western blot analysis using 6×-His Ab. For His pull-down assays, 5 μg rLvDBD was incubated with 5 μg of GST-tagged WSSV protein solution at 4°C for 3 h by agitation. Subsequently, 20 μl of the Ni-NTA binding resin were added, and the agitation continued for another 2 h. The resin was washed four times with PBS. Finally, the resins

were resuspended in 50 μl of the SDS-PAGE sample buffer, boiled, and analyzed by Western blot analysis using GST-tag Ab.

dsRNA-mediated RNA interference (RNAi)

The dsRNAs, including LvDBD and GFP, were generated by in vitro transcription with the T7 RiboMAX Express RNAi System kit (Promega) using the primers shown in Table I. The quality of dsRNA was checked by 1.5% gel electrophoresis and with a NanoDrop 2000 spectrophotometer (Thermo Fisher Scientific). The RNAi assay was performed as described previously (27). The length of LvDBD and GFP dsRNA were 378 and 504 bp, respectively. The experimental group was treated with the injection of dsRNA-LvDBD (10 μg dsRNA in each shrimp in 50 μl PBS), whereas the control groups were injected with GFP dsRNA and PBS, respectively. Gill tissues were sampled from nine shrimp samples of each challenge group at 48 h after injection and three shrimp samples pooled together, and quantitative PCR was used to investigate the RNAi efficiency.

In immune challenge experiments, after 48 h dsRNA-LvDBD injection, shrimp were injected again with 1×10^5 CFU of *V. parahaemolyticus* ($n = 30$ in each group) and 50 μl 1×10^5 copies of WSSV or PBS, respectively. The gills from each group (nine shrimp samples) were sampled for quantitative PCR to detect the relative bacterial content of *V. parahaemolyticus* or the quantification of WSSV copy number by absolute quantitative PCR. The survival

Table I. Summary of primers in this study

Primers	Sequences (5′ to 3′)
RACE	
LvDBD-5RACE1	CCAGACTCATCAGCAGGCAG
LvDBD-5RACE2	CCTTGCCTAGAACACGGATC
LvDBD-3RACE1	CCCAGGGGGTCGAGTGTTGC
LvDBD-3RACE2	GGAGAAGGGCCAGTGCCAAG
Protein expression	
LvDBD-F	GG**GAATTCC**TGCCTGCTGATGAGTCTGG
LvDBD-R	GG**CTCGAG**GAGGAAGATGCAGCACACTTCC
LvDBD-N-F	GG**GAATTC**AACATTGACAACACTCGGTTCC
LvDBD-N-R	GG**CTCGAG**GTCGGGTACTTTGTAGCAACACT
LvDBD-C-F	GG**GAATTC**AACGTGAGGGACTGCCGCG
LvDBD-C-R	GG**CTCGAG**GAGGAAGATGCAGCACACTTCCC
Quantitative PCR	
LvDBD-F	CACTCGGTTCCATCCAGAGG
LvDBD-R	CCTCACGTTGTCGGGTACTT
LvEF-1α-F	CCTATGTGCGTGGAGACCTTC
LvEF-1α-R	GCCAGATTGATCCTTCTTGTTGAC
LvDorsal-F	TTGCGACCACCAGACAAGAG
LvDorsal-R	GCAAGGTAACGACTAATCTTCTCTG
LvRelish-F	CTGCTTCTCCATACTCAGACCAC
LvRelish-R	CTGTGGCTGCTCCAGTATTTG
V. parahaemolyticus −16s-F	GGTGTAGCGGTGAAATGCGTAG
V. parahaemolyticus −16s-R	CCACAACCTCCAAGTAGACATCG
Absolute quantitative PCR	
WSSV32678-F	TGTTTTCTGTATGTAATGCGTGTAGGT
WSSV32678-R	CCCACTCCATGGCCTTCA
TaqMan probe-WSSV32706	CAAGTACCCAGGCCCAGTGTCATACGTT
dsRNA production	
dsLvDBD-F	ATGTCGACCACAATCACCCTGC
dsLvDBD-R	GAGGAAGATGCAGCACACTTCC
T7-dsLvDBD-F	GGATCCTAATACGACTCACTATAGGATGTCGACCACAATCACCCTGC
T7-dsLvDBD-R	GGATCCTAATACGACTCACTATAGGGAGGAAGATGCAGCACACTTCC
dsGFP-F	ATGGTGAGCAAGGGCGAGGAG
dsGFP-R	TTACTTGTACAGCTCGTCCATGCC
T7-dsGFP-F	GGATCCTAATACGACTCACTATAGGATGGTGAGCAAGGGCGAGGAG
T7-dsGFP-R	GGATCCTAATACGACTCACTATAGGTTACTTGTACAGCTCGTCCATGCC
dsLvDorsal-F	CTGTTGACCCACCTTACCGAC
dsLvDorsal-R	ATCTTTGACCTCATAGAAACGGAC
T7-dsLvDorsal-F	GGATCCTAATACGACTCACTATAGGCTGTTGACCCACCTTACCGAC
T7-dsLvDorsal-R	GGATCCTAATACGACTCACTATAGGATCTTTGACCTCATAGAAACGGAC
dsLvRelish-F	AGAGGTGACAGAGGTGGGAT
dsLvRelish-R	CTTGCATGGGTTATCAACTC
T7-dsLvRelish-F	GGATCCTAATACGACTCACTATAGGAGAGGTGACAGAGGTGGGAT
T7-dsLvRelish-R	GGATCCTAATACGACTCACTATAGGCTTGCATGGGTTATCAACTC
Overexpression	
LvDBD-F	GG**GAATTC**CTGCCTGCTGATGAGTCTGG
LvDBD-R	GC**TCTAGA**GAGGAAGATGCAGCACACTTCC
Genome walking	
LvDBD-F	CTTGTGTTTCGTTCGGTTATTTG
LvDBD-R	AACAAGGCTGGTGGATAAAAAAC
AP-1	GTAATACGACTCACTATAGGGC
AP-2	ACTATAGGGCACGCGTGGT
Dual-luciferase	
LvDBD-F	CC**GAGCTC**CGTAGAGTGGAGTGATGACTGACA
LvDBD-R	CC**CTCGAG**ACAAAAGCATTACTTACCAGGCAG
LvDBD-κBm-F	TGCGGTGTTCCGCTAGGTAT
LvDBD-κBm-R	ATACCTAGCGGAACACCGCA

Nucleotides in bold represent the restriction sites introduced for cloning.

rate of each group was recorded every 4 h. The Mantel-Cox (log-rank χ^2 test) method was used to analyze differences between groups using GraphPad Prism software (GraphPad Software, La Jolla, CA).

In parallel, a rescue experiment was performed to monitor the effect of rLvDBD on *V. parahaemolyticus* proliferation in vivo or survival rates after the knockdown of LvDBD in shrimp. After 48 h dsRNA-LvDBD injection, 10 μg rLvDBD was first incubated with 1×10^5 CFU of *V. parahaemolyticus* ($n = 30$ in each group) for 1 h, and then the mixture was inoculated into the experimental shrimp. The rTrx-His-tag protein was used as a control. Likewise, the bacterial content and survival rates were analyzed as above.

Absolute quantitative PCR

The quantification of WSSV copy number was detected by absolute quantitative PCR. Gills were collected from shrimp 48 h after WSSV infection. Gill DNA was extracted as described above. The concentration of WSSV genome copies was measured by absolute quantitative PCR using WSSV32678-F and WSSV32753-R primers (Table I). The PCR mixture and cycling conditions were the same as previously described (28). The WSSV genome copies were calculated and normalized to 0.1 μg of shrimp tissue DNA.

Antibacterial activity assay of rLvDBD

The minimum inhibitory concentration (MIC) was determined by a liquid growth inhibition assay as previously described with slight modifications (29). Briefly, the bacteria were inoculated into LB, cultured at 37°C until the logarithmic growth phase, and finally diluted with Poor Broth (1% w/v tryptone, 0.5% w/v NaCl, pH 7.5) to 1×10^5 CFU/ml. Serial twofold dilutions of rLvDBD ranging from 0 to 50 μM were made in the PBS buffer (10 mM Na_2HPO_4, 10 mM NaH_2PO_4, 150 mM NaCl). Then, 50 μl different concentrations of rLvDBD and 50 μl bacterial solution were added to a 96-well plate, mixed well, and incubated at 28°C for 16 h. Bacterial growth was evaluated by the culture absorbance at 600 nm measured by the ELX800 Universal Microplate Reader (Bio-Tek, Winooski, VT). Bacteria incubated with rTrx-His-tag were used as controls. Wells without bacteria were used as negative controls. If the absorbance value of the assay well is consistent with

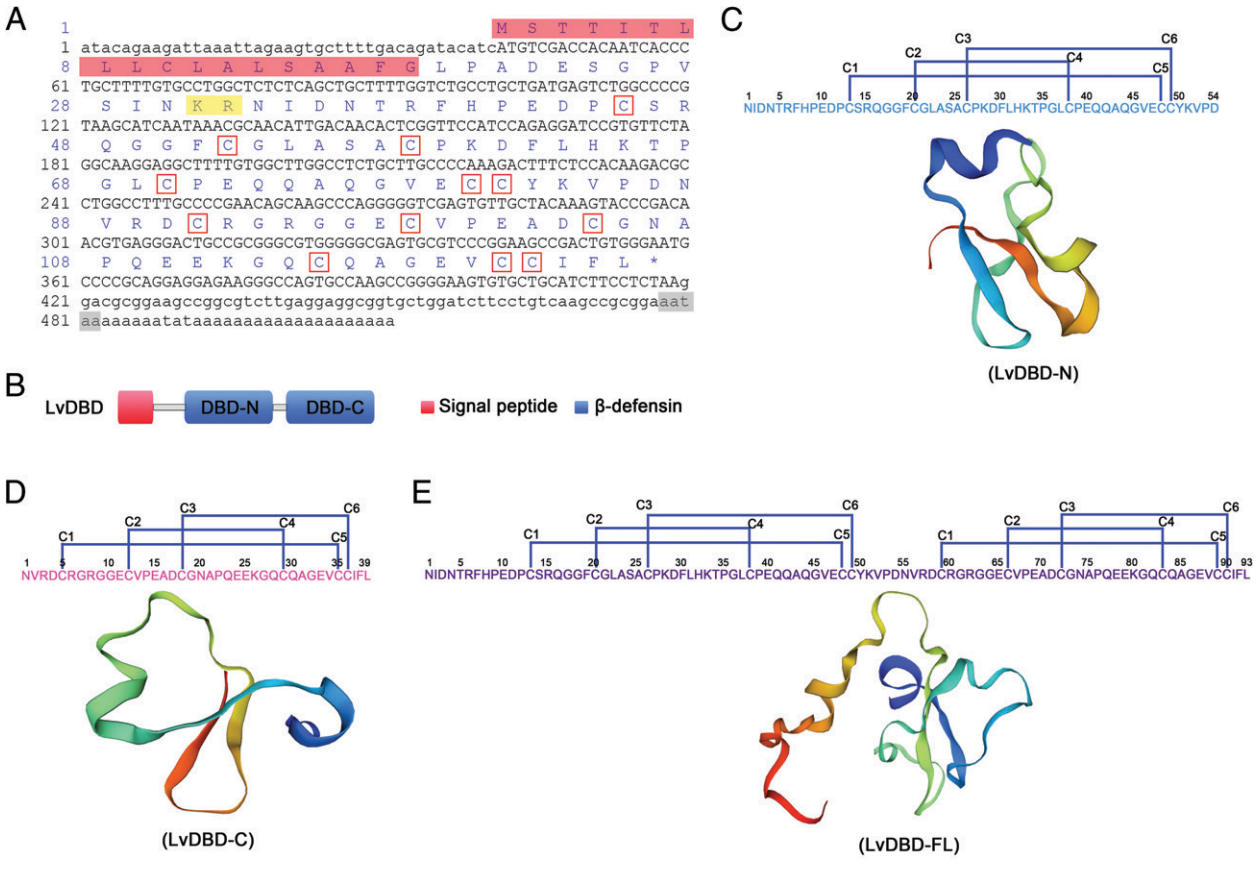

FIGURE 1. Sequence, cysteine bonding pattern, and three-dimensional structure of LvDBD. (**A**) Nucleotides and amino acids of LvDBD. The signal peptide is shaded in red, and the predicted processing site for mature peptide is shaded in yellow. The conserved cysteine residues are boxed in red, and the polyadenylation signal (aataa) is shaded in gray. (**B**) Schematic representation of the LvDBD protein. (**C–E**) Cysteine bonding pattern and predicted three-dimensional structure model of LvDBD-N (C), LvDBD-C (D), and LvDBD-FL (E). The homologous model was produced by SWISS-MODEL using the structure of *G. gallus* β-defensin 11 (SMTL ID: 6qeu.1) and *M. musculus* β-defensin 7 (SMTL ID: 1e4t.1). (**F**) Multiple sequence alignment of double-β-defensins proteins. Highly conserved amino acid residues and cysteine residues are highlighted in red.

the negative control, the minimum antimicrobial peptide concentration of its antipode is determined as the minimum antimicrobial concentration.

The detection of rLvDBD binding to bacteria

To determine the antibacterial function of rLvDBD, a bacterial binding activity assay was performed on *V. parahaemolyticus* following a previously reported method with a little modification (30). Briefly, *V. parahaemolyticus* was cultured to log phase, and the bacteria were washed with PBS buffer, then resuspended and adjusted to a final concentration of ~1×10^8 CFU/ml. A 200-μl bacterial suspension was mixed with 5 μg rLvDBD and incubated with shaking for 1 h at 25°C. The rTrx-His-tag and PBS were used as a negative control and a blank control, respectively. After incubation, the mixtures were centrifuged at 5000 rpm for 10 min, and the bacterial sediment was washed with PBS six times. Then, 300 μl of 7% SDS were added to the sediment for 10 min at 25°C, and the mixture was centrifuged at 12,000 rpm for 3 min for protein elution. Finally, the precipitates were washed with PBS six times and centrifuged at 12,000 rpm for 10 min per wash. The precipitates were prepared for SDS-PAGE and Western blot analysis.

ELISA

ELISA was used to test the microbial polysaccharide binding activity of rLvDBD, rLvDBD-N, and rLvDBD-C to LPS (from *E. coli* 055:B5; Sigma-Aldrich) and peptidoglycan (PGN) (from *S. aureus*; Sigma-Aldrich). The assays were performed as described previously (31). LPS and PGN were dissolved in distilled water at 80 μg/ml concentration, and 50 μl (4 μg) were coated to each well of the plate as previously described (32). The purified rLvDBD, rLvDBD-N, and rLvDBD-C were diluted in TBS to different concentrations: 0.01, 0.1, 0.25, 0.5, 0.75, and 1.0 μM. The plates were incubated with the recombinant protein for 3 h at 25°C and then washed with TBS four times and incubated with mouse anti-His mAb (1:2000 dilution in TBS with 0.1 μg/μl BSA) for 1 h at 37°C. Plates were washed four times with binding buffer (200 μl/well) and then 100 μl HRP-conjugated anti-mouse IgG (1:2000 dilution in TBS with 0.1 mg/ml BSA) for 1 h at 37°C. After the plates were washed again four times with binding buffer, the color reaction was developed by 3,3′,5,5′ -tetramethylbenzidine liquid substrate in citric acid-Na_2HPO_4 buffer (0.01%) and then stopped by adding 2 M H_2SO_4. The absorbance was read at 450 nm using a plate reader (Bio-Tek). K_d, the ligand concentration when half of the receptor was bound by the ligand, was used to assess the affinity of rLvDBD to polysaccharide. K_d was calculated using GraphPad Prism 5 with nonlinear regression curve fit and one-site binding model analysis. The binding assays were repeated three times.

Phagocytosis analysis

The phagocytosis analysis was performed according to a previously reported method (33). Hemocytes were collected from shrimp, washed with 2× Leibovitz L-15 medium (Thermo Fisher Scientific) three times, counted using a BD Accuri C6 flow cytometer (BD Biosciences, San Jose, CA), and stained with Dil (Beyotime Biotechnology, Shanghai, China), then incubated at 25°C for 20 min. After three washes with L-15 medium, the hemocytes were mixed with 5 μg rLvDBD, rLvDBD-N, and rLvDBD-C (or PBS and rTrx as controls) together with FITC-labeled *V. parahaemolyticus* and incubated 25°C for 1 h. After three washes with L-15 medium, hemocytes were detected using flow cytometry, and the Dil and FITC double-fluorescence signals were used to identify cells that had phagocytized bacteria. The thresholds and boundaries of fluorescence signals were set on the basis of detection of the control Dil-stained hemocytes and FITC-labeled *V. parahaemolyticus* phagocytized by unstained cells. A total of 100,000 events were detected for each sample.

Transmission electron microscopy (TEM) observation

The effect of rLvDBD treatment on *V. parahaemolyticus* was observed using TEM. The treatment method used to obtain the suspension of bacteria was the same as that in a previous study (18). The bacteria were cultured to the appropriate concentration and incubated at 25°C with an equal volume of rLvDBD, rLvDBD-N, and rLvDBD-C (final concentration of 50 μM) for 2 h.

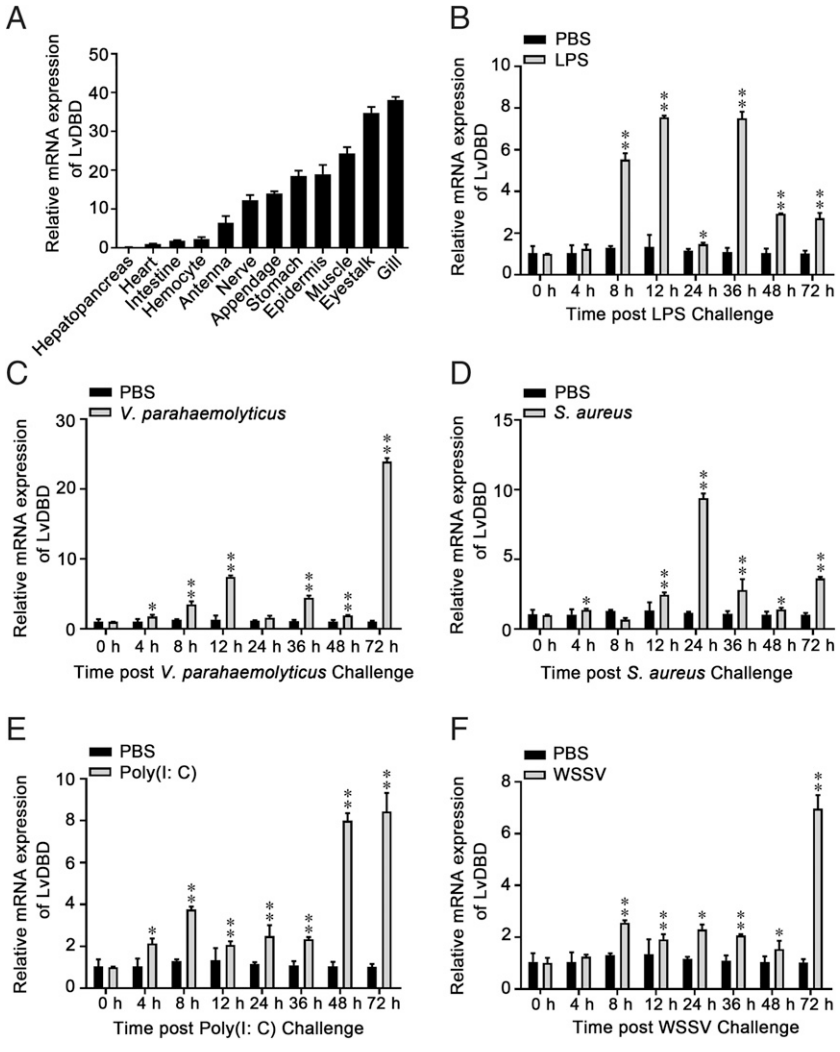

FIGURE 2. Tissue distribution and expression profiles of LvDBD. (**A**) The transcription levels of LvDBD in different tissues of healthy shrimp. The expression level in the hepatopancreas was used as a control and set to 1.0. (**B**–**F**) The expression profiles of LvDBD in gills from LPS (B)-, *V. parahaemolyticus* (C)-, *S. aureus* (D)-, polyinosinic-polycytidylic acid [Poly (I:C)] (E)-, or WSSV (F)-challenged shrimp. Expression values were normalized to those of *EF-1α* by using the Livak ($2^{-\Delta\Delta CT}$) method. The statistical significance was calculated using Student *t* test (**$p < 0.01$, *$p < 0.05$). All experiments were performed three times and yielded similar results.

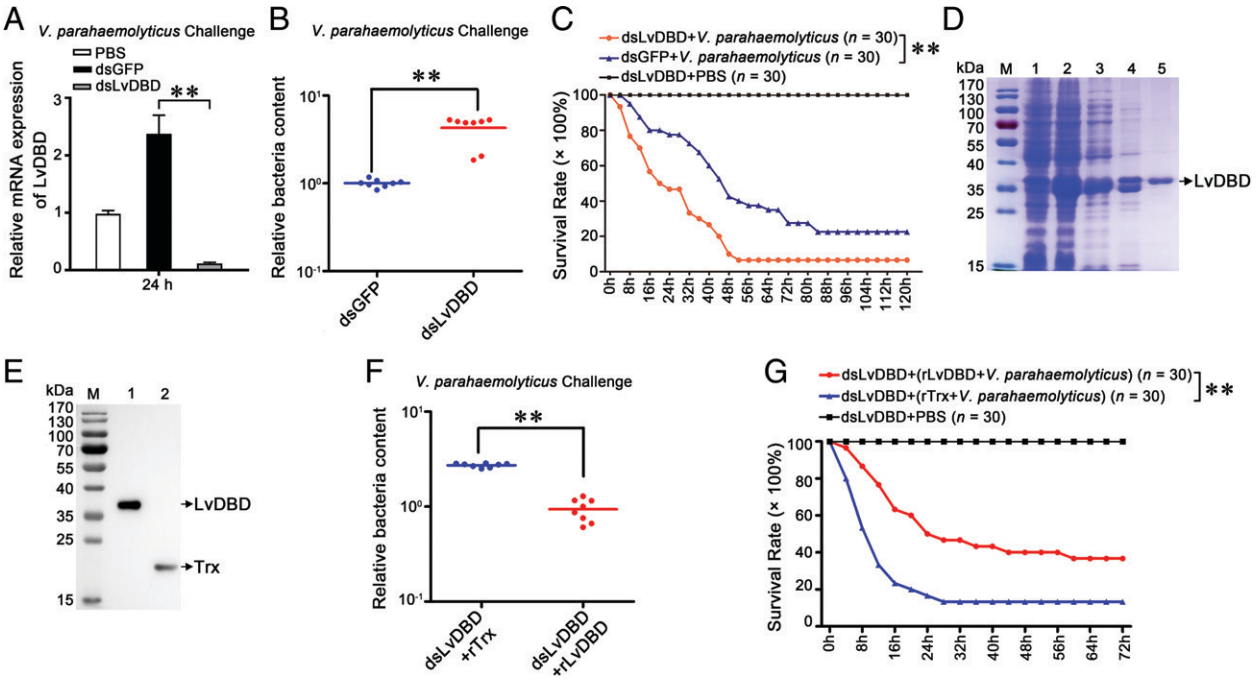

FIGURE 3. Potent antibacterial activities of LvDBD against *V. parahaemolyticus*. (**A**) The silencing efficiency of LvDBD in gills 24 h after *V. parahaemolyticus* infection. (**B**) The relative bacterial loads in gills from each group (eight shrimp samples) at 24 h after infection. (**C**) Shrimp survival rates following treatment with dsRNAs and experimental infection with *V. parahaemolyticus*. (**D**) SDS-PAGE analysis of the recombinant LvDBD protein expressed in *E. coli*. Line 1, uninduced *E. coli* transformed with LvDBD; line 2, induced *E. coli* transformed with LvDBD; line 3, supernatant of ultrasonic lysed *E. coli* expressing LvDBD; line 4, precipitate of lysed *E. coli* expressing LvDBD; line 5, purified recombinant LvDBD protein (black arrow). (**E**) Purified rLvDBD and rTrx-His-tag proteins were checked by Western blotting with anti-6×-His Ab. (**F**) The relative bacterial loads in gills from each group (eight shrimp samples) in rescue experiments. At 48 h after dsRNA injection, the shrimp samples were injected with *V. parahaemolyticus* premixed with purified rLvDBD. (**G**) Shrimp survival rates in rescue experiments. At 48 h after dsRNA injection, the shrimp were injected with *V. parahaemolyticus* premixed with purified rLvDBD or rTrx-His-tag. The survival rates of shrimp were recorded every 4 h to calculate the survival rate by using the Kaplan-Meier method (**$p < 0.01$). All experiments were performed three times and yielded similar results.

PBS or rTrx-His tag was used as a control. The bacterial pellets were fixed with 2.5% glutaraldehyde in 1× PBS overnight at 4°C and washed three times with PBS. After being washed with distilled water three times, the samples were counterstained with 2% sodium phosphotungstate for 1 min and then observed by TEM (JEM-100CXII, JEOL, Tokyo, Japan).

Dual-luciferase reporter assays

The partial promoter sequence with 155 bp upstream of LvDBD was cloned using the specific primers (Table I) and then linked into pGL3-Basic (Promega) to generate pGL3-κB (reporter plasmid). The vector pGL3-kBm, containing 155-bp promoters of LvDBD with deletion mutant of the NF-κB binding motif (TGGAATTTCCA), was also generated. The *L. vannamei* Dorsal and Relish expression vectors (pAc-LvDorsal-V5 and pAc-LvRelsih-V5) were obtained from our previous studies (34, 35). Because no permanent shrimp cell line was available, the *Drosophila* Schneider 2 (S2) cell line (ATCC CRL-1963) was used instead to detect the effects of *L. vannamei* NF-κB on the promoters of LvDBD. S2 cells were cultured at 28°C in Schneider's Insect Medium (Sigma-Aldrich) containing 10% FBS (Life Technologies, Grand Island, NY). For dual-luciferase reporter assays, S2 cells were plated into a 96-well plate, and 12 h later, the cells of each well were transfected with 0.05 μg of firefly luciferase reporter gene plasmids, 0.001 μg pRL-TK Renilla luciferase plasmid (Promega), or 0.05 μg protein expression plasmids or empty pAc5.1A plasmids (as controls) using FuGENE HD Transfection Reagent (Promega) according to the user manual. Forty-eight hours after transfection, the dual-luciferase reporter assays were performed to calculate the relative ratios of firefly and Renilla luciferase activities using the Dual-Glo Luciferase Assay System kit (Promega) according to the manufacturer's instructions. All experiments were repeated six times.

Coimmunoprecipitation

Coimmunoprecipitation assays in vitro were performed to confirm interaction between LvDBD and VP19, VP24, VP26, and VP28. After 48-h transfection, *Drosophila* S2 cells were harvested and washed with ice-cold PBS three times and then lysed in immunoprecipitated lysis buffer with Halt Protease Inhibitor Cocktail (Thermo Fisher Scientific). The supernatants (400 μl) were incubated with 30 μl of anti-Flag magnetic beads (Bimake, Shanghai, China) or anti-hemagglutinin magnetic beads (Thermo Fisher Scientific) at 25°C for 30 min. The magnetic beads were washed with PBS six times and subjected to SDS-PAGE assay. Five percent of each total cell lysate was also examined as the input control.

Statistical analysis

All data are presented as mean ± SD. The Student *t* test was used to calculate the comparisons between groups of numerical data. For survival rates, data were subjected to statistical analysis using GraphPad Prism software (GraphPad Software) to generate the Kaplan-Meier plots (log-rank χ^2 test).

Results

LvDBD is a member of the double-β-defensin family

The transcript of LvDBD (accession no. ON081627) has a length of 511 bp and consists of a 41-bp 5′-untranslated region (UTR), a 92-bp 3′-UTR containing a single polyadenylation signal (AATAA), and a 378-bp open reading frame, which encodes a protein of 125 aa with a calculated molecular mass of 13.31 kDa (Table I). The precursor

Table II. Antimicrobial activity of purified LvDBD peptide

Microorganisms	MIC (μM)
Gram-negative bacteria	
Vibrio parahaemolyticus	12.5
Aeromonas hydrophila	50
Pseudomonas aeruginosa	25
Escherichia coli	25
Gram-positive bacteria	
Enterococcus faecalis	25
Staphylococcus aureus	25
Micrococcus luteus	25
Bacillus subtilis	25

MIC is defined as the lowest protein concentration harvesting visible growth inhibition function compared with the negative control.

peptide of LvDBD contained a signal peptide of 18 residues and two β-defensin domains with 12 conserved cysteines, namely, the N-terminal and C-terminal β-defensin domains. The predicted mature peptide cleavage sites were Lys (K31) and Arg (R32) (Fig. 1A, 1B). Both the LvDBD-N and LvDBD-C domains contained six conserved cysteines with typical disulfide array (Cys1–Cys5, Cys2–Cys4, and Cys3–Cys6; Fig. 1C, 1D). By using the structure of defensin proteins from *M. musculus* (SMTL ID: 1e4t.1) and *G. gallus* (SMTL ID: 6qeu.1) as templates to perform the homologous modeling, we found that LvDBD-C revealed high homology similarity to *M. musculus* β-defensin 7, whereas LvDBD-N and LvDBD-FL had significant homology similarity to *Gga-AvBD11* (Fig. 1C, 1E). Multiple sequence analysis showed that the double-β-defensin motif is highly conserved with 12 conservative cysteine residues among different members in vertebrates and arthropods (Fig. 1F). According to the neighbor-joining phylogenetic tree, the double-β-defensin homologs from various species could be divided into two groups, namely, the vertebrate group and another group that contains LvDBD and others from arthropods (Supplemental Fig. 1). The results suggest that LvDBD is a member of the double-β-defensin family.

LvDBD was induced in immune-challenged shrimp

Tissue distribution analysis showed that LvDBD was expressed highly in the gills, muscle, and eyestalk with 38.15-fold, 34.80-fold, and 24.34-fold levels, respectively, over that in the hepatopancreas (set to 1.0) (Fig. 2A). We next explored whether LvDBD is involved in the immune response to a series of stimuli in the gills. In response to LPS challenge, the expression of LvDBD was abruptly upregulated at 8 h (5.53-fold), 12 h (7.56-fold), and 36 h (7.51-fold), then slightly downregulated at 48 h (2.93-fold) and 72 h (2.72-fold; Fig. 2B). After infection with *V. parahaemolyticus*, the expression of LvDBD was dramatically upregulated at 12 h with a 7.47-fold increase, then slightly downregulated at 24 h (1.62-fold), and finally abruptly upregulated at 72 h (23.94-fold; Fig. 2C). After infection with *S. aureus*,

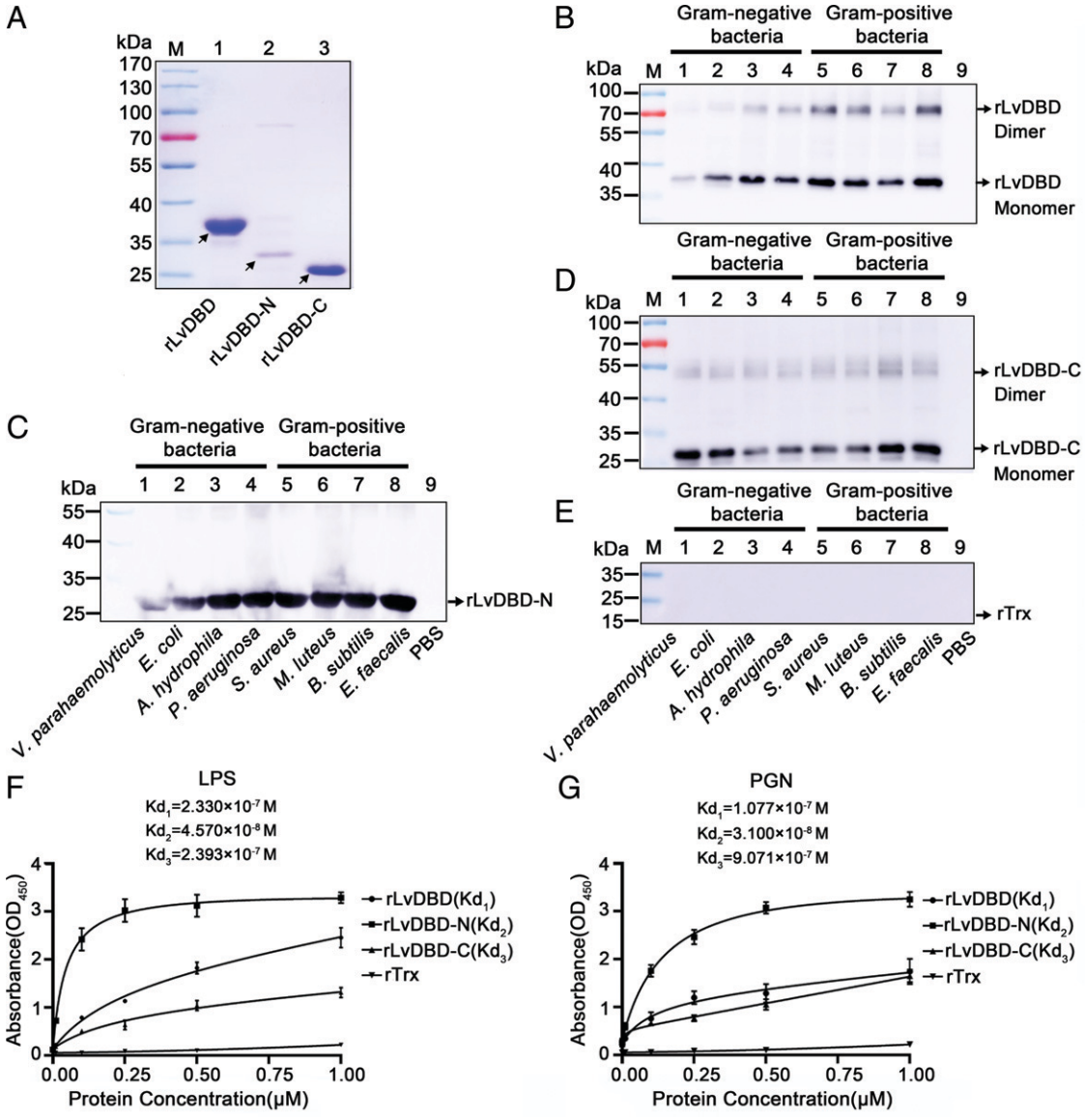

FIGURE 4. LvDBD binds to bacteria and polysaccharides. (**A**) Recombinant expression and purification of LvDBD (line 1), LvDBD-N (line 2), and LvDBD-C (line 3). These purified proteins were analyzed using SDS-PAGE and stained with Coomassie blue. (**B**–**E**) Bacterial binding activities of rLvDBD (B), rLvDBD-N (C), rLvDBD-C (D), and rTrx (E). Lines 1–4 represent the Gram-negative bacteria, including *V. parahaemolyticus*, *E. coli*, *A. hydrophila*, and *P. aeruginosa*. Lines 5–8 represent the Gram-positive bacteria, including *S. aureus*, *M. luteus*, *B. subtilis*, and *E. faecalis*. Line 9 represents PBS. (**F**, **G**) The dissociation constants of recombinant LvDBD protein–polysaccharide complexes. The solid lines denote the rLvDBD (K_{d1}), rLvDBD-N (K_{d2}), and rLvDBD-C (K_{d3}) binding ability to LPS (F) and PGN (G). The rTrx protein was used as a negative control. All experiments were performed three times and yielded similar results.

the expression of LvDBD was induced at different time points with a peak (9.39-fold) at 24 h (Fig. 2D). After injection of polyinosinic-polycytidylic acid, the expression of LvDBD was upregulated at 36 h and remained high at 48 h (8.01-fold) and 72 h (8.45-fold; Fig. 2E). After infection with WSSV, the expression of LvDBD was dramatically induced at 8 h (2.57-fold), 24 h (2.30-fold), and 72 h (6.97-fold; Fig. 2F). Therefore, LvDBD expression was induced in response to pathogen inoculation and immune stimulus treatment.

LvDBD played a critical role in defense against V. parahaemolyticus *infection*

To explore the function of LvDBD during *V. parahaemolyticus* infection, we knocked down LvDBD expression in vivo via RNAi. First, we designed and synthesized the dsRNA, namely dsLvDBD, which can specifically target LvDBD. At 48 h after dsRNA injection, shrimp samples were injected with *V. parahaemolyticus* or PBS, and their survival numbers were counted every 4 h. The silencing efficiency of LvDBD was checked by quantitative PCR at 24 h after *V. parahaemolyticus* infection. The mRNA level of LvDBD was effectively suppressed by the specific dsLvDBD in gills, and the value was downregulated to 0.05-fold of the dsGFP injection group (as a control) (Fig. 3A). Meanwhile, the relative bacterial content of the dsLvDBD group was considerably higher than that of the control group, showing a 4.29-fold increase (Fig. 3B). In addition, the survival rate of shrimp in the LvDBD-silenced group was significantly lower than that in the GFP-knockdown group ($p < 0.01$; Fig. 3C).

To further demonstrate the actual role of LvDBD, we performed in vivo RNAi experiments coupled with rLvDBD injection. The recombinant proteins of rLvDBD and rTrx-His-tag were expressed, purified by SDS-PAGE gels, and checked by Coomassie staining (Fig. 3D), and the results were further confirmed by Western blot analysis (Fig. 3E). After knockdown of the endogenous LvDBD, shrimp samples were treated with *V. parahaemolyticus* mixed with rLvDBD or rTrx-His-tag by i.m. injection. Consequently, the relative bacterial content of the samples coinjected with rLvDBD was significantly reduced compared with that of the control group ($p < 0.01$; Fig. 3F). In addition, the survival rates of shrimp coinjected with rLvDBD were significantly higher than those of the control group ($p < 0.01$; Fig. 3G). Therefore, LvDBD plays a crucial role in the immune defense against *V. parahaemolyticus* infection in vivo.

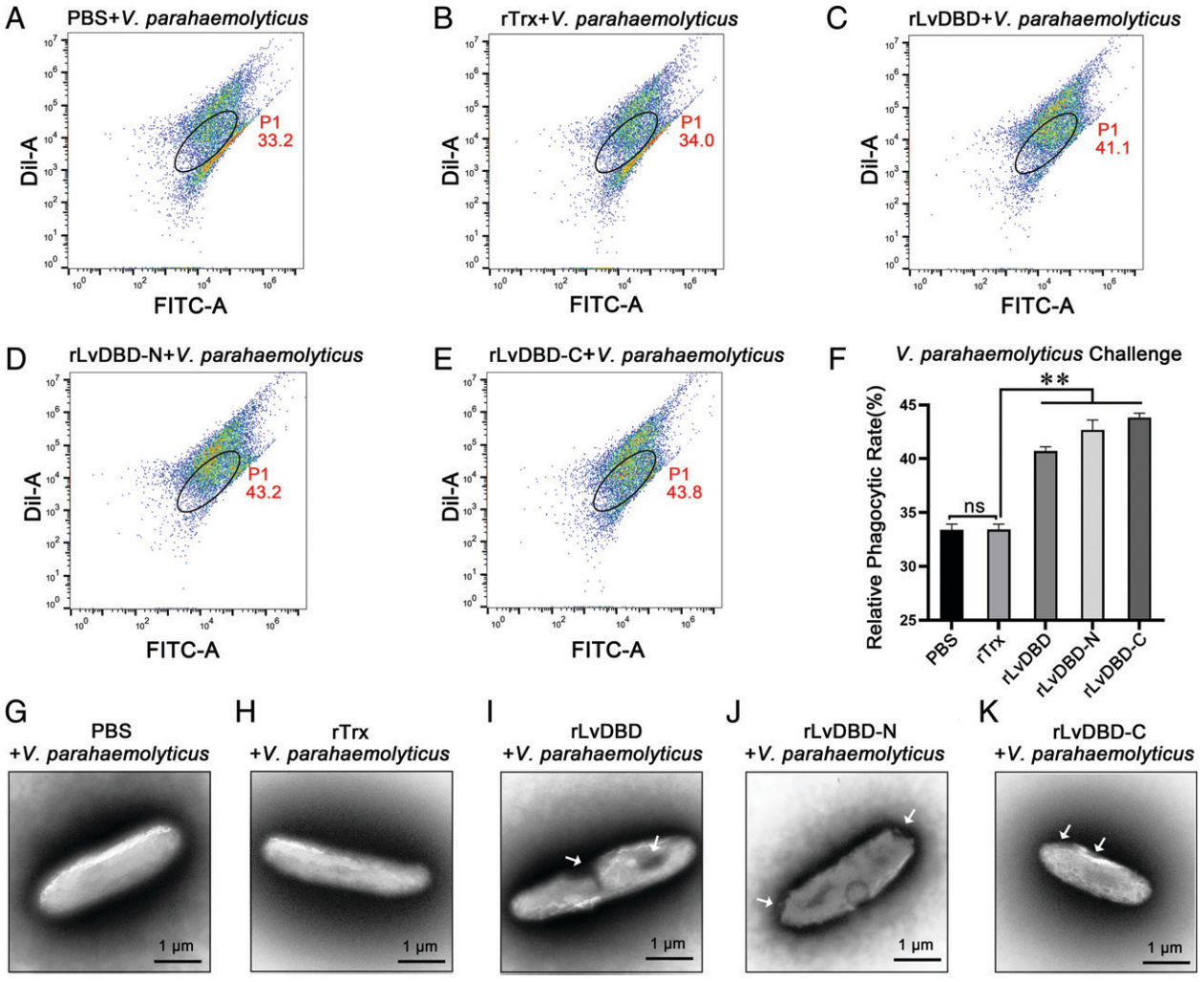

FIGURE 5. Hemocyte phagocytosis activities of LvDBD toward *V. parahaemolyticus*. (**A**–**E**) The influence of rLvDBD (C), rLvDBD-N (D), and rLvDBD-C (E) proteins on the hemocyte phagocytosis activities. PBS (A) and rTrx-Tag (B) were used as controls. (**F**) Statistical analysis of the relative hemocyte phagocytosis. The results are representative of three injection experiments with data presented as mean ± SD of three parallel detections. All data were analyzed statistically by Student *t* test (**$p < 0.01$, *$p < 0.05$). (**G**–**K**) TEM images of *V. parahaemolyticus* treated with rLvDBD (I), rLvDBD-N (J), and rLvDBD-C (K) proteins. PBS (G) and rTrx-Tag (H) were used as controls. *V. parahaemolyticus* was incubated with recombinant protein at 28°C, and the images showed the morphology and structure of *V. parahaemolyticus* by TEM examination. White arrows show the damaged *V. parahaemolyticus* membrane. Scale bar, 1 μm. All experiments were performed three times and yielded similar results.

Microbial and polysaccharide binding activities of LvDBD

To test the antimicrobial activity of rLvDBD, we performed liquid growth inhibition assays in vitro. The MICs against Gram-positive or -negative bacteria for rLvDBD are listed in Table II. On the basis of MIC values, rLvDBD showed superior inhibitory abilities against *V. parahaemolyticus*, *P. aeruginosa*, and *E. coli*. However, rLvDBD showed a little inhibitory ability against *A. hydrophila* with an MIC value of 50 μM. The MIC values for Gram-positive bacteria (*E. faecalis*, *S. aureus*, *M. luteus*, and *B. subtilis*) were all 25 μM (Table II).

To further explore the antibacterial mechanism of LvDBD, we expressed and purified the proteins of rLvDBD (full length), rLvDBD-N, and rLvDBD-C (Fig. 4A and Supplemental Fig. 2). Microorganism binding assays were carried out by Western blot analysis. The results showed that rLvDBD and rLvDBD-C could strongly bind to all these tested Gram-negative bacteria (*V. parahaemolyticus*, *E. coli*, *A. hydrophila*, and *P. aeruginosa*) and Gram-positive bacteria (*S. aureus*, *M. luteus*, *B. subtilis*, and *E. faecalis*) in both monomer and dimer patterns (Fig. 4B, 4D). By contrast, the rLvDBD-N was bound to these Gram-negative and -positive bacteria in a monomeric form (Fig. 4C). In the control group, rTrx-His-tag could not bind to either Gram-negative or -positive bacteria (Fig. 4E). The C-terminal defensin domain of LvDBD conferred dimerization activity. To clarify whether the microbial binding ability of rLvDBD was mediated by bacterial surface polysaccharides, we used ELISA to detect the binding capacity of rLvDBD, rLvDBD-N, and rLvDBD-C toward LPS and PGN. The K_d of rLvDBD (K_{d1}), rLvDBD-N (K_{d2}), and rLvDBD-C (K_{d3}) toward LPS, which were calculated on the basis of saturation curve, were 2.330×10^{-7}, 4.570×10^{-8}, and 2.393×10^{-7} M, respectively (Fig. 4F). The K_{d1}, K_{d2}, and K_{d3} values toward PGN were 1.007×10^{-7}, 3.110×10^{-8}, and 9.071×10^{-7} M, respectively (Fig. 4G). The results showed that rLvDBD-N has a stronger binding ability than rLvDBD and rLvDBD-C to LPS and PGN. Therefore, LvDBD has a potential antibacterial activity with ability to bind to bacteria, LPS, and PGN.

LvDBD enhanced the phagocytosis of hemocytes toward V. parahaemolyticus

The effect of LvDBD on hemocyte phagocytic activity against FITC-labeled *V. parahaemolyticus* was analyzed by flow cytometry by using purified rLvDBD, rLvDBD-N, and rLvDBD-C. Hemocytes that have phagocytized FITC-labeled bacteria were identified by Dil and FITC double-fluorescence signals, in which the analysis gate was set on the basis of detection of the controls (Supplemental Fig. 3). The results showed that rLvDBD (Fig. 5C), rLvDBD-N (Fig. 5D), and rLvDBD-C (Fig. 5E) increased the phagocytosis activity compared with PBS (Fig. 5A) or rTrx (Fig. 5B) tag. Specifically, the relative phagocytosis rates of hemocytes preincubated with rLvDBD (41.1%), rLvDBD-N (43.2%), and rLvDBD-C (43.8%) were significantly increased compared with those of PBS (33.2%) and rTrx (34.0%; Fig. 5F). To further investigate the effect of LvDBD on bacterial microstructure, we observed the morphological and structural changes of *V. parahaemolyticus* cells before and after incubation with rLvDBD, rLvDBD-N, and rLvDBD-C under TEM. The bacterial cells from the PBS-treated group (Fig. 5G) and the rTrx-His-tag-treated group (Fig. 5H) had normal shapes with complete architecture, and the outer membrane was round and smooth. However, the bacterial cells displayed a rough and cracked appearance in

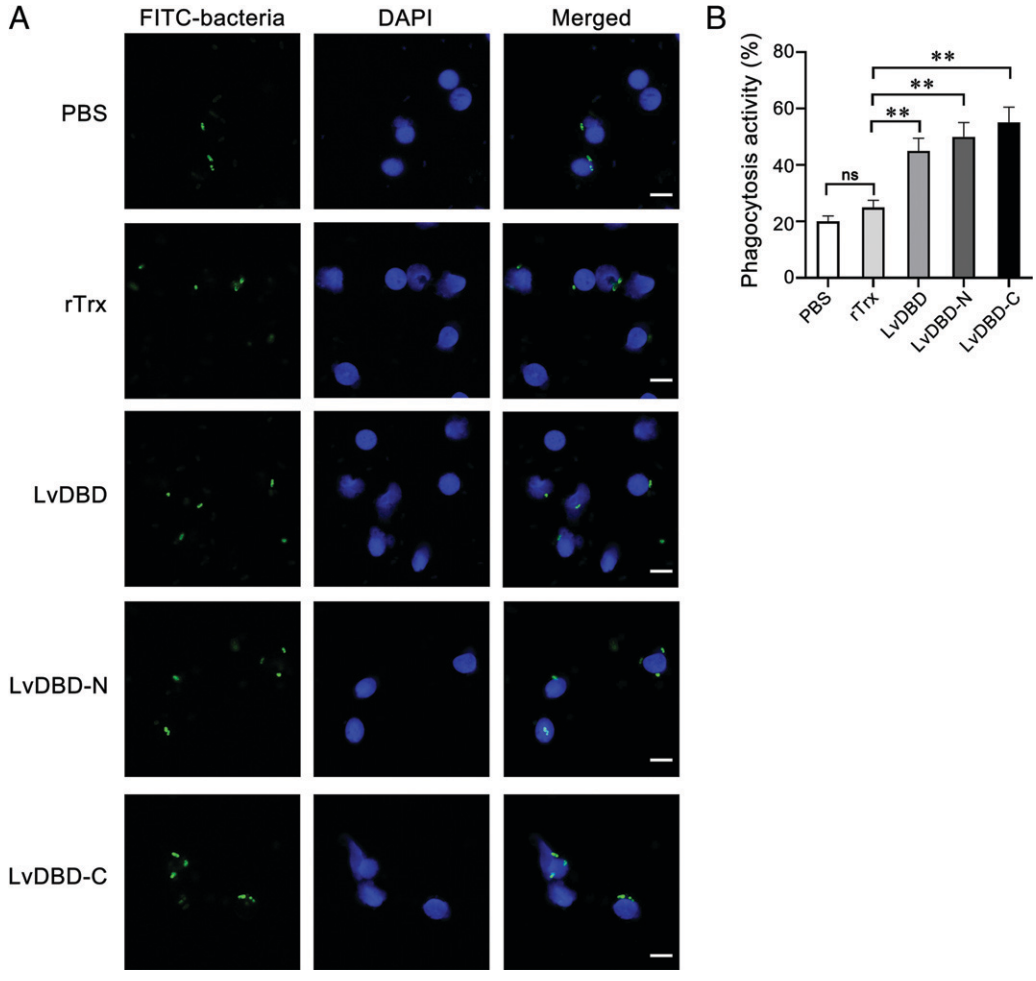

FIGURE 6. Phagocytosis activity of hemocytes toward bacteria was promoted by rLvDBD. (**A**) Recombinant rLvDBD, rLv DBD-N, and rLvDBD-C proteins were incubated with FITC-labeled *V. parahaemolyticus* (green) and then added to hemocytes for 1 h. Cells were fixed and subsequently stained with DAPI (blue) to label the nuclei. PBS and rTrx were used as controls. Scale bar, 25 μm. (**B**) Statistical analysis of the phagocytosis rate of hemocytes. The phagocytosis rate was calculated as (hemocytes ingesting bacteria/all hemocytes observed or tested) × 100%. The statistical significance was calculated using Student *t* test (**$p < 0.01$). The results are derived from three independent repeats.

rLvDBD (Fig. 5I)-, rLvDBD-N (Fig. 5J)-, and rLvDBD-C (Fig. 5K)-treated groups. In addition, hemocyte phagocytosis was observed under the fluorescence microscope, and the results demonstrated that LvDBD could promote hemocyte phagocytosis (Fig. 6A, 6B). Therefore, LvDBD could cause rupture of the outer membrane of *V. parahaemolyticus* and positively regulate the phagocytosis of hemocytes toward them as well.

LvDBD inhibited WSSV replication and interacted with WSSV envelope proteins

RNAi was also used to gain insight into the role of LvDBD during WSSV infection. At 48 h after dsRNA injection, shrimp samples were injected with WSSV. The silencing efficiency of LvDBD was checked by quantitative PCR at 48 h after WSSV infection. The results show that the mRNA level of LvDBD was effectively suppressed by the specific dsRNA in gills, which was downregulated to 0.11-fold of the GFP dsRNA injection group (as a control; Fig. 7A). The quantities of WSSV copies in the gills of the dsLvDBD group were significantly higher than those of the control group, with a 3.75-fold increase, on average (Fig. 7B). To clarify the possible antiviral mechanism of LvDBD, we performed pull-down assays to detect whether rLvDBD protein could interact with WSSV envelope proteins. The main envelope proteins of WSSV, including VP19, VP24, VP26, and VP28 with GST tags, were expressed and purified and then confirmed by Western blot analysis with the GST-tag Ab (Fig. 7C). In the GST-tagged pull-down assays, rLvDBD could interact with VP19, VP24, VP26, and VP28 by SDS-PAGE gels based on Coomassie blue staining (Fig. 7D), and results were further confirmed by Western blot analysis with the 6×-His Ab (Fig. 7E). On the basis of His-tagged pull-down assays, VP19, VP24, VP26, and VP28 could precipitate rLvDBD (Fig. 7F), and this result was further confirmed by Western blot analysis with GST Ab (Fig. 7G). The interactions between LvDBD and WSSV envelope proteins were also evidenced by immunoprecipitation assay by using ectopic expression of these proteins in *Drosophila* S2 cells (Supplementary Fig. 4A, 4B). Therefore, LvDBD could inhibit WSSV replication and bind to VP19, VP24, VP26, and VP28 (Fig. 7H).

LvDBD was regulated by conserved NF-κB pathway

In the shrimp *L. vannamei*, Dorsal and Relish (NF-κB), the downstream transcription factors of Toll and IMD signaling pathways were crucial factors to induce the production of antimicrobial peptides in response to pathogen invasion (12). To determine whether Dorsal and Relish regulated the expression of LvDBD in vitro, we performed a dual-luciferase reporter assay in *Drosophila* S2 cells. We cloned the promoter region of LvDBD by genome walking, and this region contains putative conserved κB motifs located at −110 to −100 (κB, TGGAATTTCCA; Fig. 8A). Then, the reporter assay results showed that the ectopic expression of Dorsal and Relish (Fig. 8B) remarkably improved the promoter activity of pGL3-κB (Fig. 8C), whereas the activity of pGL3-κBm was not upregulated (Fig. 8D). Then, we determined whether the expression of LvDBD was regulated by Dorsal and Relish in vivo by performing an RNAi experiment. The mRNA levels of LvDBD remarkably decreased

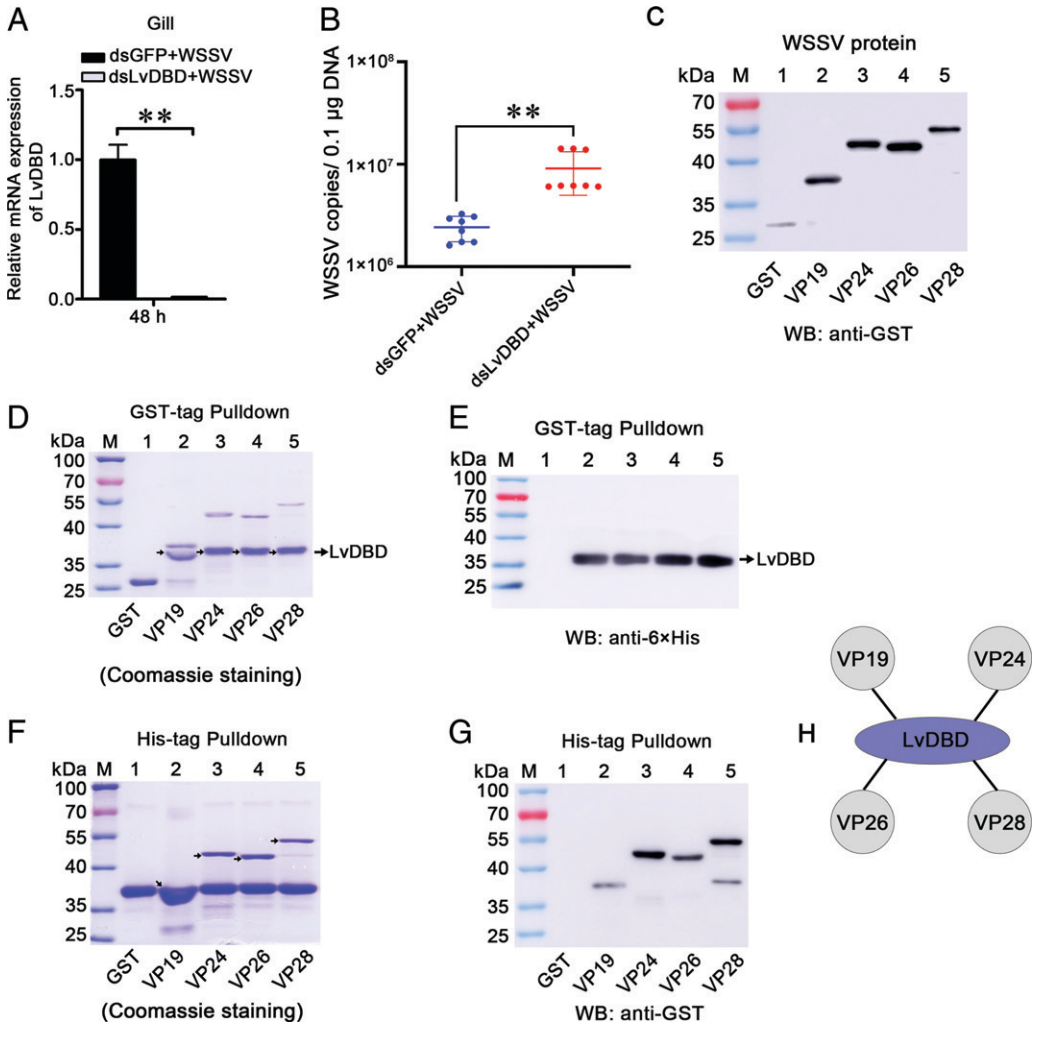

FIGURE 7. LvDBD interacted with envelope proteins of WSSV. (**A**) The silencing efficiency of LvDBD in gills 48 h after WSSV infection. (**B**) The quantity of WSSV copies in gills from each group (eight shrimp samples) at 48 h postinfection. (**C**) The purified recombinant proteins of GST, GST-tagged VP19, VP24, VP26, and VP28, were confirmed by Western blotting. (**D** and **E**) GST pull-down assay for the detection of the interaction between rLvDBD with VP19, VP24, VP26, and VP28. The results were shown via staining with Coomassie blue (D) or Western blotting using 6×-His Ab (E). The GST-tag protein was used as a control. (**F** and **G**) His pull-down assay for the detection of the interaction of rLvDBD with VP19, VP24, VP26, and VP28 via Coomassie blue staining (F) or Western blotting using the GST-tag Ab (G). The GST-tag protein was used as a control. (**H**) Schematic illustrations of the interaction of LvDBD with VP19, VP24, VP26, and VP28. The statistical significance was calculated using Student *t* test (**$p < 0.01$). All experiments were repeated three times and yielded similar results.

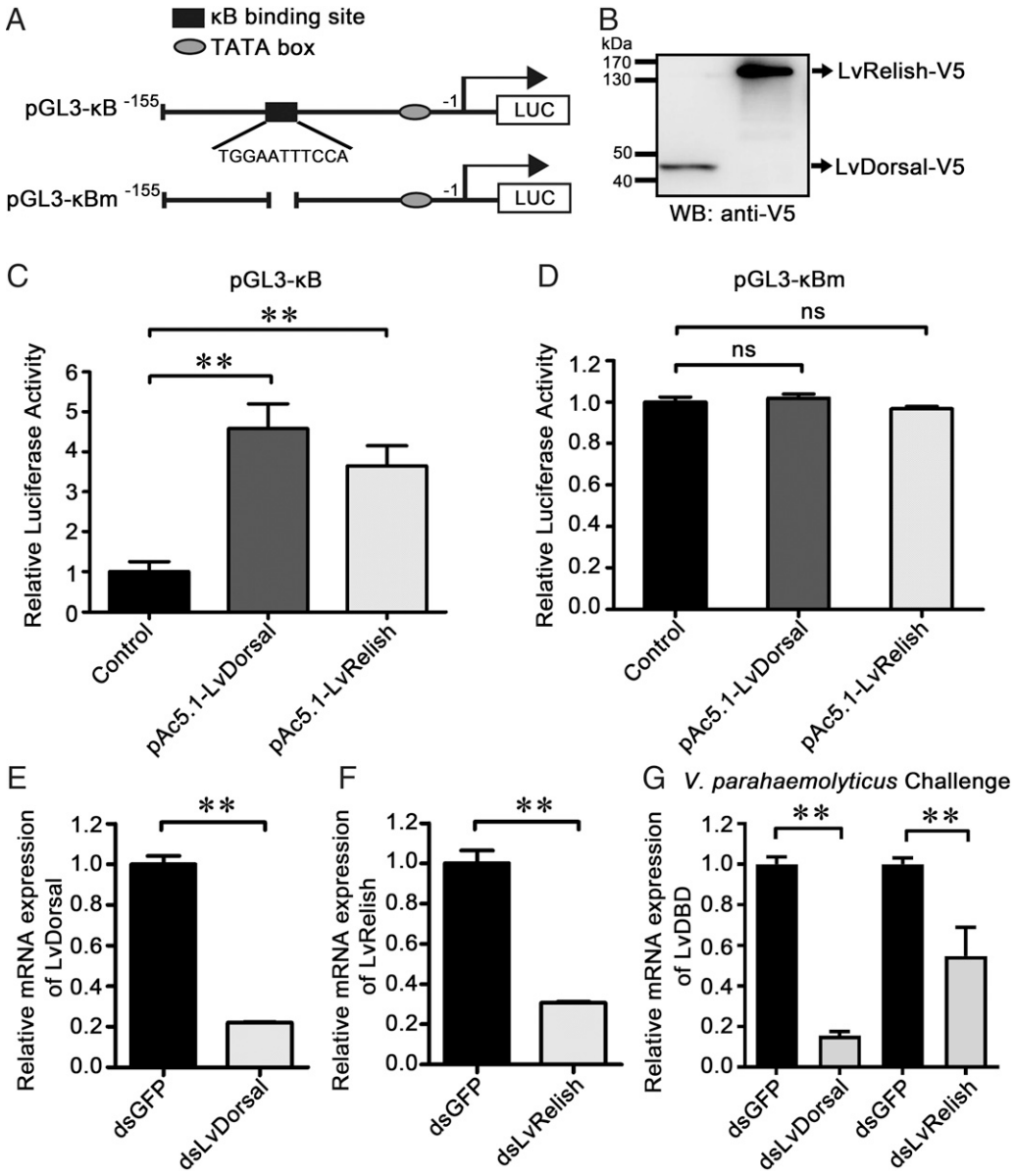

FIGURE 8. Activation of the LvDBD promoter by shrimp NF-κB. (**A**) Schematic diagram of the LvDBD promoter regions in the luciferase reporter gene constructs. The deletion mutant of the NF-κB binding motif site of the LvDBD promoter was shown in absolute value sign; the wild type is shown in black rectangle; and TATA box is shown in elliptical shape. The −1 indicates 1 bp before the translation initiation site. LUC denoted the firefly luciferase reporter gene. (**B**) Ectopic expression of LvDorsal and LvRelish in *Drosophila* S2 cells was detected with anti-V5 Ab. (**C**) Dual-luciferase reporter assays were performed to analyze the effects of the overexpression of Dorsal and Relish on the promoter activities of LvDBD in *Drosophila* S2 cells. The value of cells transfected with an empty plasmid (pAc5.1/V5-His A), which were used as a control and set as 1.0, is shown. (**D**) Dual-luciferase reporter assays were performed to analyze the effects of the overexpression of Dorsal and Relish on the promoter activities of LvDBD with mutated NF-κB binding motif. (**E** and **F**) Effective knockdown for LvDorsal (E) and LvRelish (F) in hemocytes by dsRNA was confirmed by quantitative PCR. (**G**) The mRNA levels of LvDBD in the hemocytes of LvDorsal- and LvRelish-silenced shrimp under *V. parahaemolyticus* challenge. The statistical significance was calculated using Student *t* test (**$p < 0.01$). All experiments were repeated three times and yielded similar results.

in the gills of Dorsal- or Relish-silenced shrimp during *V. parahaemolyticus* infection (Fig. 8E, 8F), confirming that the expression of LvDBD was regulated by NF-κB in shrimp (Fig. 8G). Therefore, Dorsal and Relish could regulate the expression of LvDBD in vitro and in vivo (Fig. 9).

Discussion

Antimicrobial peptides, as the first line of defense against invading pathogens, are crucial components of nonspecific innate immunity (36). β-Defensins, which are a type of conserved host defense peptide, are found in all the vertebrate genomes sequenced, demonstrating that this gene family originated very early in vertebrate evolution (37). However, the presence of defensins or defensin-like peptides with two β-defensin motifs is rarely reported in vertebrates and invertebrates. An atypical double-β-defensin from *G. gallus* (*Gga*-AvBD11) has recently been identified (9), whereas the avian double-β-defensin family has been described in quail (38), turkey (39), green lizard *Anolis carolinensis* (40, 41), and Komodo dragon (42) but has not been found in other animal classes. In this study, we identified a double−β-defensin-like peptide from an invertebrate, the shrimp *L. vannamei* (named LvDBD), and clarified its antimicrobial function toward both

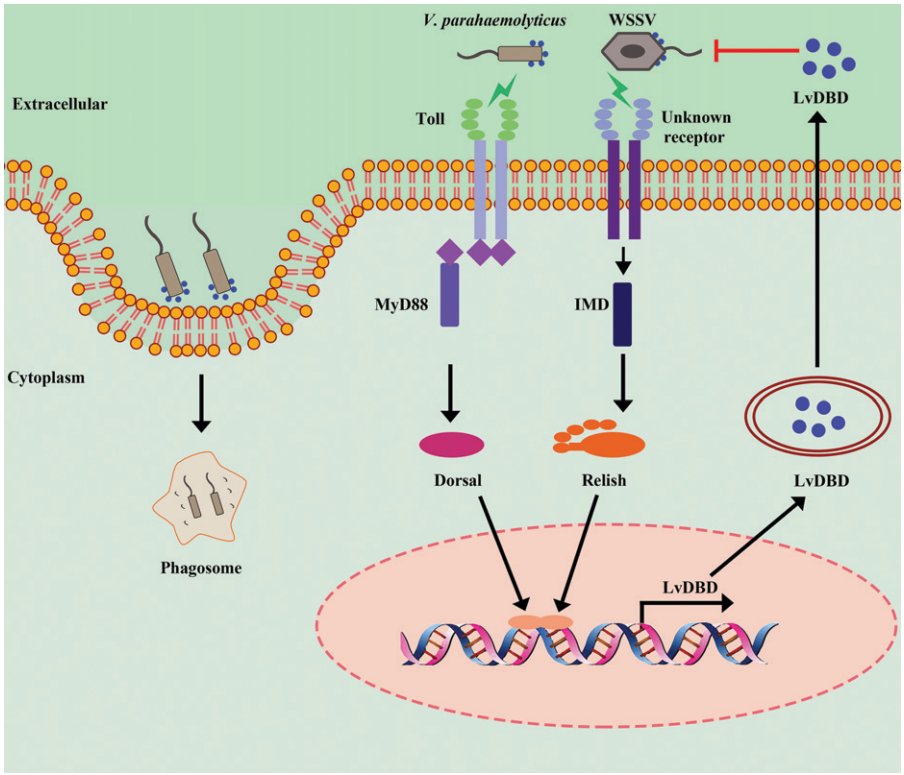

FIGURE 9. Model for LvDBD-mediated antibacterial and antiviral mechanism against *V. parahaemolyticus* and WSSV. *V. parahaemolyticus* and WSSV infection resulted in the activation of host Dorsal and Relish (NF-κB) signaling pathways that triggered the synthesis and secretion of LvDBD. The secreted LvDBD exhibited strong binding activities to *V. parahaemolyticus* and enhanced the phagocytosis activity of hemocytes to *V. parahaemolyticus*. In addition, the LvDBD could inhibit WSSV infection by interacting with its envelope proteins, including VP19, VP24, VP26, and VP28.

bacteria and virus, which extended the discovery and functional understanding of a double-β-defensin to an invertebrate.

We extensively analyzed the sequence homologies related to LvDBD by screening a series of sequences from vertebrates and invertebrates containing two β-defensin domains. The 12 cysteines, including their disulfide bond arrangements and two glycine units, were completely conserved among the 21 analyzed double-β-defensin members, although the overall sequence identities between LvDBD and the other homologs are less than 42% (Fig. 1F). This large variability in the sequences is a well-known feature of defensins, where only cysteines ensuring the disulfide bridge arrangements and the rare glycine residues that are required for the appropriate three-dimensional structure resist the high adaptive genetic variation during evolution (9). The genomic plasticity of defense coding sequences is conducive to fostering the adaptability of the innate immune system and enables the acquisition of new functions, such as the venomous vertebrate β-defensin, which have evolved to target ion channels of their prey (43). Double-β-defensin is presumed to originate from the duplication and fusion of an ancestral monodomain β-defensin gene during the evolution of arthropods (9). The evolutionary origin of LvDBD is of research interest because a monodomain β-defensin gene has not been found after searching the shrimp *L. vannamei* genome and transcriptome.

The remarkably increased expression of LvDBD in response to *V. parahaemolyticus* infection implied its potential critical role in defense against this intrusive pathogen. The RNAi-mediated knockdown of LvDBD in vivo led to phenotypes with higher bacterial loads and rendered shrimp more susceptible to *V. parahaemolyticus* infection, whereas the purified rLvDBD could reduce the bacterial loads and rescue survival rate. Besides, LvDBD has a wide range of antibacterial activity against multiple Gram-positive and -negative bacteria. The independent or synergistic functions of the two isolated β-defensin domains of LvDBD have not been fully determined, although some information is provided in the present work. The LvDBD-C domain is responsible for the dimerization of LvDBD, which may contribute to the stability of mature peptide. However, the dimerization could not be implicated with the binding ability of bacterial polysaccharides, because LvDBD-N had strong binding activities toward polysaccharides (LPS and PGN). During evolution, the emergence of such a double-domain β-defensin should be driven by its increased biological potency compared with a single-domain molecule, and then new functions carried only by the full-length protein should be acquired (9). Among the bird double-β-defensins, *Gga*-AvBD11 has been identified against Gram-positive and -negative bacteria, parasites, and some viruses (9, 11). The antibacterial activity of AvDBD is mainly mediated by its N-terminal domain, but the antiviral activity requires the full-length protein (9). Thus, further work is needed to improve the understanding of the independent or synergistic functions of the two isolated β-defensin domains of LvDBD.

Defensins, including α-, β-, and θ-defensin, have antiviral activity against both enveloped and nonenveloped viruses (44). Direct interactions between defensins and viral envelope or capsid could disrupt virus–receptor interactions (45), disturb viral fusion (46), and inhibit viral entry into target cells (47). Interestingly, LvDBD binds all the four main envelope proteins, including VP19, VP24, VP26, and VP28. Notably, almost all defensins are cationic antimicrobial peptides (7, 48). Sequence analysis reveals that the N-terminal of LvDBD consists of five positively charged amino acid residues (three lysine residues [Lys60, Lys65, Lys83] and two arginine residues [Arg38, Arg47]) exhibiting the properties of cationic amino acids. We noted that the four envelope proteins contain a series of aspartate and glutamate negatively charged residues, namely, Asp81, Asn82, Asp83, Asp84, Glu85, and Asp86, in VP19; Asp180, Glu181, Asp182, Ile183, Asp184, and Asp185 in VP24; Asp196, Ile197, Lys198, Asp199, and Glu200 in VP26; and Ile163, Asp164, Glu165, Asp166, and Glu167 in VP28. Therefore, LvDBD would interact with them via electrostatic interaction. However, the mechanism in which LvDBD interacts with these envelope proteins should be further investigated. VP19, VP24, VP26, and VP28 play a crucial role during WSSV infection (49). Especially, WSSV envelope proteins VP24, VP26, and VP28 interact with one another to form a complex termed an

"infectosome," which is crucial to the infectivity of WSSV (50, 51). Therefore, LvDBD could interact with WSSV envelope proteins, which could disrupt WSSV integrity and attenuate viral entry into the shrimp cells.

Antimicrobial peptides function as the specific effectors for microbial infection, and they are produced and regulated by the immune signaling pathway, especially the Toll and IMD signaling pathways (12, 52, 53). The determination of the specific pathway that is responsible for the transcriptional expression of LvDBD in shrimp will improve the understanding of the immune response to pathogen invasion. In shrimp, both NF-κB transcription factors (Dorsal and Relish), the downstream transcription factors of Toll and IMD pathways, participate in the transcriptional expression of a series of antimicrobial peptides in response to bacterial and viral infection (26, 54, 55). In the present study, LvDBD was regulated by both NF-κB transcription factors (Dorsal and Relish) that used the same κB motif in its promoter, indicating that its expression could respond to both Toll and IMD pathways. A similar circumstance was observed in *Drosophila*, in which a single κB motif in the promoter of Metchnikowin was regulated by both Dif and Relish (56). Notably, the induction of LvDBD expression by Dorsal and Relish suggests the presence of a signaling crosstalk between the Toll and IMD pathways in shrimp.

In conclusion, we functionally identified a double-β-defensin from an arthropod, the shrimp *L. vannamei*. On the basis of our results, we proposed a model for the function of LvDBD in the innate immunity in shrimp (Fig. 9). In response to *V. parahaemolyticus* and WSSV infection, shrimp Toll/IMD-NF-κB signaling pathways were activated to induce the expression of LvDBD via an NF-κB-responsive element in its promoter. The secreted LvDBD that was bound to the bacteria, probably via bacterial surface polysaccharides LPS and PGN, and interacted with WSSV, probably via VPs, resulted in a lower infectivity of the virus or bacteria. Besides, LvDBD could contribute to host clearance of bacteria via phagocytosis, although its biological function in phagocytosis has not been fully clarified. It is not clear how effective this would be as an antibiotic, but the data do confirm that LvDBD has an important role in protecting shrimp from the bacteria and virus. Together, the functional identification of LvDBD not only provides some insights into the understanding of the double-β-defensin in invertebrates but also facilitates the development of antimicrobial agents for bacterial and viral diseases in shrimp aquaculture.

Acknowledgments

We thank LetPub (www.letpub.com) for linguistic assistance during the preparation of the manuscript.

Disclosures

The authors have no financial conflicts of interest.

References

1. Gwyer Findlay, E., S. M. Currie, and D. J. Davidson. 2013. Cationic host defence peptides: potential as antiviral therapeutics. *BioDrugs* 27: 479–493.
2. Zasloff, M. 2019. Antimicrobial peptides of multicellular organisms: my perspective. *Adv. Exp. Med. Biol.* 1117: 3–6.
3. Zhao, B. R., Y. Zheng, J. Gao, and X. W. Wang. 2020. Maturation of an antimicrobial peptide inhibits *Aeromonas hydrophila* infection in crayfish. *J. Immunol.* 204: 487–497.
4. Brogden, K. A. 2005. Antimicrobial peptides: pore formers or metabolic inhibitors in bacteria? *Nat. Rev. Microbiol.* 3: 238–250.
5. Glukhov, E., M. Stark, L. L. Burrows, and C. M. Deber. 2005. Basis for selectivity of cationic antimicrobial peptides for bacterial versus mammalian membranes. *J. Biol. Chem.* 280: 33960–33967.
6. Dhople, V., A. Krukemeyer, and A. Ramamoorthy. 2006. The human beta-defensin-3, an antibacterial peptide with multiple biological functions. *Biochim. Biophys. Acta* 1758: 1499–1512.
7. Meade, K. G., and C. O'Farrelly. 2019. β-defensins: farming the microbiome for homeostasis and health. *Front. Immunol.* 9: 3072.
8. Vu, G. H., D. Do, C. D. Rivera, P. S. Dickinson, A. E. Christie, and E. A. Stemmler. 2018. Characterization of the mature form of a β-defensin-like peptide, Hoa-D1, in the lobster *Homarus americanus*. *Mol. Immunol.* 101: 329–343.
9. Guyot, N., H. Meudal, S. Trapp, S. Iochmann, A. Silvestre, G. Jousset, V. Labas, P. Reverdiau, K. Loth, V. Hervé, et al. 2020. Structure, function, and evolution of *Gga*-AvBD11, the archetype of the structural avian-double-β-defensin family. *Proc. Natl. Acad. Sci. USA* 117: 337–345.
10. Guyot, N., C. Landon, and P. Monget. 2022. The two domains of the avian double-β-defensin AvBD11 have different ancestors, common with potential monodomain crocodile and turtle defensins. *Biology (Basel)* 11: 690.
11. Hervé-Grépinet, V., S. Réhault-Godbert, V. Labas, T. Magallon, C. Derache, M. Lavergne, J. Gautron, A. C. Lalmanach, and Y. Nys. 2010. Purification and characterization of avian beta-defensin 11, an antimicrobial peptide of the hen egg. *Antimicrob. Agents Chemother.* 54: 4401–4409.
12. Li, C., S. Wang, and J. He. 2019. The two NF-κB pathways regulating bacterial and WSSV infection of shrimp. *Front. Immunol.* 10: 1785.
13. De Schryver, P., T. Defoirdt, and P. Sorgeloos. 2014. Early mortality syndrome outbreaks: a microbial management issue in shrimp farming? *PLoS Pathog.* 10: e1003919.
14. Escobedo-Bonilla, C. M., V. Alday-Sanz, M. Wille, P. Sorgeloos, M. B. Pensaert, and H. J. Nauwynck. 2008. A review on the morphology, molecular characterization, morphogenesis and pathogenesis of white spot syndrome virus. *J. Fish Dis.* 31: 1–18.
15. Van Etten, J. 2009. Lesser known large dsDNA viruses. Preface. *Curr. Top. Microbiol. Immunol.* 328: v–vii.
16. Cabello, F. C., H. P. Godfrey, A. H. Buschmann, and H. J. Dölz. 2016. Aquaculture as yet another environmental gateway to the development and globalisation of antimicrobial resistance. *Lancet Infect. Dis.* 16: e127–e133.
17. Su, H., S. Liu, X. Hu, X. Xu, W. Xu, Y. Xu, Z. Li, G. Wen, Y. Liu, and Y. Cao. 2017. Occurrence and temporal variation of antibiotic resistance genes (ARGs) in shrimp aquaculture: ARGs dissemination from farming source to reared organisms. *Sci. Total Environ.* 607-608: 357–366.
18. Xiao, B., X. Liao, H. Wang, J. He, and C. Li. 2021. BigPEN, an antimicrobial peptide of penaeidin family from shrimp *Litopenaeus vannamei* with membrane permeable and DNA binding activity. [Published erratum appears in 2022 *Fish Shellfish Immunol. Rep.* 3: 100050.] *Fish Shellfish Immunol. Rep.* 2: 100034.
19. Li, C., S. Weng, Y. Chen, X. Yu, L. Lü, H. Zhang, J. He, and X. Xu. 2012. Analysis of *Litopenaeus vannamei* transcriptome using the next-generation DNA sequencing technique. *PLoS One* 7: e47442.
20. Wang, S., B. Yin, H. Li, B. Xiao, K. Lǔ, C. Feng, J. He, and C. Li. 2018. MKK4 from *Litopenaeus vannamei* is a regulator of p38 MAPK kinase and involved in anti-bacterial response. *Dev. Comp. Immunol.* 78: 61–70.
21. Schultz, J., F. Milpetz, P. Bork, and C. P. Ponting. 1998. SMART, a simple modular architecture research tool: identification of signaling domains. *Proc. Natl. Acad. Sci. USA* 95: 5857–5864.
22. Artimo, P., M. Jonnalagedda, K. Arnold, D. Baratin, G. Csardi, E. de Castro, S. Duvaud, V. Flegel, A. Fortier, E. Gasteiger, et al. 2012. ExPASy: SIB bioinformatics resource portal. *Nucleic Acids Res.* 40: W597–W603.
23. Li, H., Q. Fu, S. Wang, R. Chen, X. Jiang, P. Zhu, J. He, and C. Li. 2020. TNF-receptor-associated factor 3 in *Litopenaeus vannamei* restricts white spot syndrome virus infection through the IRF-Vago antiviral pathway. *Front. Immunol.* 11: 2110.
24. Waterhouse, A., M. Bertoni, S. Bienert, G. Studer, G. Tauriello, R. Gumienny, F. T. Heer, T. A. P. de Beer, C. Rempfer, L. Bordoli, et al. 2018. SWISS-MODEL: homology modelling of protein structures and complexes. *Nucleic Acids Res.* 46: W296–W303.
25. Li, H., S. Wang, K. Lǔ, B. Yin, B. Xiao, S. Li, J. He, and C. Li. 2017. An invertebrate STING from shrimp activates an innate immune defense against bacterial infection. *FEBS Lett.* 591: 1010–1017.
26. Xiao, B., Q. Fu, S. Niu, P. Zhu, J. He, and C. Li. 2020. Penaeidins restrict white spot syndrome virus infection by antagonizing the envelope proteins to block viral entry. *Emerg. Microbes Infect.* 9: 390–412.
27. Li, H., S. Wang, Y. Chen, K. Lǔ, B. Yin, S. Li, J. He, and C. Li. 2017. Identification of two p53 isoforms from *Litopenaeus vannamei* and their interaction with NF-κB to induce distinct immune response. *Sci. Rep.* 7: 45821.
28. Wang, S., H. Li, S. Weng, C. Li, and J. He. 2020. White spot syndrome virus establishes a novel IE1/JNK/c-Jun positive feedback loop to drive replication. *iScience* 23: 100752.
29. Imjongjirak, C., P. Amparyup, and A. Tassanakajon. 2011. Two novel antimicrobial peptides, arasin-likeSp and GRPSp, from the mud crab *Scylla paramamosain*, exhibit the activity against some crustacean pathogenic bacteria. *Fish Shellfish Immunol.* 30: 706–712.
30. Zhang, H., W. Cheng, L. Zheng, P. Wang, Q. Liu, Z. Li, T. Li, Y. Wei, Y. Mao, and X. Yu. 2020. Identification of a group D anti-lipopolysaccharide factor (ALF) from kuruma prawn (*Marsupenaeus japonicus*) with antibacterial activity against *Vibrio parahaemolyticus*. *Fish Shellfish Immunol.* 102: 368–380.
31. Shi, X. Z., X. Zhong, and X. Q. Yu. 2012. *Drosophila melanogaster* NPC2 proteins bind bacterial cell wall components and may function in immune signal pathways. *Insect Biochem. Mol. Biol.* 42: 545–556.
32. Qin, N., H. Sun, M. Lu, J. Wang, T. Tang, and F. Liu. 2020. A single von Willebrand factor C-domain protein acts as an extracellular pattern-recognition receptor in the river prawn *Macrobrachium nipponense*. *J. Biol. Chem.* 295: 10468–10477.
33. Zuo, H., K. Weng, M. Luo, L. Yang, S. Weng, J. He, and X. Xu. 2020. A microRNA-1-mediated inhibition of the NF-κB pathway by the JAK-STAT pathway in the invertebrate *Litopenaeus vannamei*. *J. Immunol.* 204: 2918–2930.
34. Huang, X. D., Z. X. Yin, X. T. Jia, J. P. Liang, H. S. Ai, L. S. Yang, X. Liu, P. H. Wang, S. D. Li, S. P. Weng, et al. 2010. Identification and functional study of a shrimp Dorsal homologue. *Dev. Comp. Immunol.* 34: 107–113.

35. Huang, X. D., Z. X. Yin, J. X. Liao, P. H. Wang, L. S. Yang, H. S. Ai, Z. H. Gu, X. T. Jia, S. P. Weng, X. Q. Yu, and J. G. He. 2009. Identification and functional study of a shrimp Relish homologue. *Fish Shellfish Immunol.* 27: 230–238.
36. Mahlapuu, M., J. Håkansson, L. Ringstad, and C. Björn. 2016. Antimicrobial peptides: an emerging category of therapeutic agents. *Front. Cell. Infect. Microbiol.* 6: 194.
37. Zou, J., C. Mercier, A. Koussounadis, and C. Secombes. 2007. Discovery of multiple beta-defensin like homologues in teleost fish. *Mol. Immunol.* 44: 638–647.
38. Rahman, M. A., A. Moriyama, A. Iwasawa, and N. Yoshizaki. 2009. Cuticle formation in quail eggs. *Zool. Sci.* 26: 496–499.
39. Mann, K., and M. Mann. 2013. The proteome of the calcified layer organic matrix of turkey (*Meleagris gallopavo*) eggshell. *Proteome Sci.* 11: 40.
40. Dalla Valle, L., F. Benato, S. Maistro, S. Quinzani, and L. Alibardi. 2012. Bioinformatic and molecular characterization of beta-defensins-like peptides isolated from the green lizard *Anolis carolinensis*. *Dev. Comp. Immunol.* 36: 222–229.
41. Fry, B. G., K. Roelants, K. Winter, W. C. Hodgson, L. Griesman, H. F. Kwok, D. Scanlon, J. Karas, C. Shaw, L. Wong, and J. A. Norman. 2010. Novel venom proteins produced by differential domain-expression strategies in beaded lizards and gila monsters (genus *Heloderma*). *Mol. Biol. Evol.* 27: 395–407.
42. van Hoek, M. L., M. D. Prickett, R. E. Settlage, L. Kang, P. Michalak, K. A. Vliet, and B. M. Bishop. 2019. The Komodo dragon (*Varanus komodoensis*) genome and identification of innate immunity genes and clusters. *BMC Genomics* 20: 684.
43. Whittington, C. M., A. T. Papenfuss, P. W. Kuchel, and K. Belov. 2008. Expression patterns of platypus defensin and related venom genes across a range of tissue types reveal the possibility of broader functions for OvDLPs than previously suspected. *Toxicon* 52: 559–565.
44. Holly, M. K., K. Diaz, and J. G. Smith. 2017. Defensins in viral infection and pathogenesis. *Annu. Rev. Virol.* 4: 369–391.
45. Hazrati, E., B. Galen, W. Lu, W. Wang, Y. Ouyang, M. J. Keller, R. I. Lehrer, and B. C. Herold. 2006. Human alpha- and beta-defensins block multiple steps in herpes simplex virus infection. *J. Immunol.* 177: 8658–8666.
46. Demirkhanyan, L., M. Marin, W. Lu, and G. B. Melikyan. 2013. Sub-inhibitory concentrations of human α-defensin potentiate neutralizing antibodies against HIV-1 gp41 pre-hairpin intermediates in the presence of serum. *PLoS Pathog.* 9: e1003431.
47. Wilson, S. S., M. E. Wiens, and J. G. Smith. 2013. Antiviral mechanisms of human defensins. *J. Mol. Biol.* 425: 4965–4980.
48. Sørensen, O. E., N. Borregaard, and A. M. Cole. 2008. Antimicrobial peptides in innate immune responses. *Contrib. Microbiol.* 15: 61–77.
49. Zhou, Q., L. Xu, H. Li, Y. P. Qi, and F. Yang. 2009. Four major envelope proteins of white spot syndrome virus bind to form a complex. *J. Virol.* 83: 4709–4712.
50. Chang, Y. S., W. J. Liu, C. C. Lee, T. L. Chou, Y. T. Lee, T. S. Wu, J. Y. Huang, W. T. Huang, T. L. Lee, G. H. Kou, et al. 2010. A 3D model of the membrane protein complex formed by the white spot syndrome virus structural proteins. *PLoS One* 5: e10718.
51. Li, Z., W. Chen, L. Xu, F. Li, and F. Yang. 2015. Identification of the interaction domains of white spot syndrome virus envelope proteins VP28 and VP24. *Virus Res.* 200: 24–29.
52. Clemmons, A. W., S. A. Lindsay, and S. A. Wasserman. 2015. An effector peptide family required for *Drosophila* Toll-mediated immunity. *PLoS Pathog.* 11: e1004876.
53. Li, C., S. Weng, and J. He. 2019. WSSV-host interaction: host response and immune evasion. *Fish Shellfish Immunol.* 84: 558–571.
54. Li, H., B. Yin, S. Wang, Q. Fu, B. Xiao, K. Lǔ, J. He, and C. Li. 2018. RNAi screening identifies a new Toll from shrimp *Litopenaeus vannamei* that restricts WSSV infection through activating Dorsal to induce antimicrobial peptides. *PLoS Pathog.* 14: e1007109.
55. Wang, S., H. Li, R. Chen, X. Jiang, J. He, and C. Li. 2022. TAK1 confers antibacterial protection through mediating the activation of MAPK and NF-κB pathways in shrimp. *Fish Shellfish Immunol.* 123: 248–256.
56. Busse, M. S., C. P. Arnold, P. Towb, J. Katrivesis, and S. A. Wasserman. 2007. A kappaB sequence code for pathway-specific innate immune responses. *EMBO J.* 26: 3826–3835.